"This document is the Accepted Manuscript version of a Published Work that appeared in final form in Journal of Materials Chemistry A, copyright © The Royal Society of Chemistry 2019 after peer review and technical editing by the publisher. To access the final edited and published work see:

https://pubs.rsc.org/en/content/articlelanding/2019/ta/c9ta08818k#!divAbstract

Multi-layered photocathodes based on $Cu_2ZnSnSe_4$ absorber and MoS_2 catalyst for the Hydrogen Evolution Reaction

Received 00th January 20xx,
Accepted 00th January 20xx

DOI: 10.1039/x0xx00000x

Sergi Grau,[a] Sergio Giraldo,[b] Edgardo Saucedo,[b] Joan Ramón Morante,[b] Antoni Llobet*[a,c] and Carolina Gimbert-Suriñach*[a]

A multilayered p-type photoabsorber based on kesterite $Cu_2ZnSnSe_4$ has been functionalized with inexpensive and easily scalable amorphous MoS_2 electrocatalyst by cathodic photoelectrodeposition. The resulting photocathodes with a final composition of Mo/$MoSe_2$/$Cu_2ZnSnSe_4$/CdS/ZnO/ITO/MoS_2 (where ITO = indium tin oxide) feature one of the highest hydrogen evolution catalytic current density reported to date at a potential E = 0 V vs RHE (-18 mA/cm^2 in pH 2) under 1 sun illumination. A comparison of the performance of the photoelectrode with an analogous dark electrode with composition ITO/MoS_2 allows us to estimate a photovoltage of 430 mV, which is very close to the working voltage of an equivalent photovoltaic cell with open circuit voltage V_{OC} = 464 mV. The photoelectrodes show sustained activity at -10 mA/cm^2 above the thermodynamic potential of the H^+/H_2 redox couple (E = +86 mV) for 1 hour without any loss of activity. Prolonged reaction times up to 4 hours show no degradation of the photoabsorber multilayered architecture but a decrease in the thickness of the the MoS_2 electrocatalytic film due to the mechanical stress caused by the hydrogen bubbles forming on the surface of the electrode. The MoS_2 layer is key not only to catalyze the catalytic reaction but also to protect the photoabsorber from the corrosive electrolyte solution. The adhesion of the MoS_2 electrocatalytic film on the ITO top layer is critical for the stability during hydrogen evolution catalysis.

Introduction

Since 2000 the worldwide energy consumption has been increasing with an average rate of 2.3 % with contaminating fossil fuels being one the main primary source.[1,2] Thus, finding sources of energy, that are renewable, environmentally friendly and that can supply our energy demand is imperative.

Artificial photosynthesis is a general term used to describe the light induced reactions that promote the oxidation of water to dioxygen and use the generated reducing equivalents to transform aqueous protons to hydrogen gas or reduce CO_2 to useful carbon based fuels.[3,4] One common strategy for the hydrogen production in the context of artificial photosynthesis is the use of a photoelectrochemical cell (PEC), where one or two photoelectrodes harvest the light and generate electron-hole pairs that are used to perform the oxygen evolution reaction (OER, photoanode) and hydrogen evolution reaction (HER, photocathode). An example of a simple PEC based on a photocatode and a dark anode is given in Figure 1.[5-8] Thermodynamically, the water splitting reaction requires 1.23 V (WS, eq. 1) but in practice, an additional overpotential associated with the kinetic barriers of each half-reaction is needed (HER in eq. 2 and OER in eq. 3). To minimize the overpotential required for the HER and OER it's necessary to use selective and efficient catalysts for each reaction.

Platinum is the best catalyst for HER known to date, able to reduce protons to molecular hydrogen with almost no overpotential, but is scarce and expensive.[9,10] A cheaper and remarkably well-performing material is MoS_2, which was not investigated as a HER catalyst due to its low activity as bulk material until 2005, when Nørskov and co-workers demonstrated that MoS_2 nanoparticles are in fact very active.[12] Further experimental and theoretical studies revealed that the morphology and size of the nanoparticles are critical for the catalytic performance and that only the edge sites and sulfur vacancies are the active sites on the crystallographic edges.[12,13,14] Since then, numerous studies with different synthetic approaches to obtain MoS_2 active for HER with different crystalline nanostructures as well as amorphous MoS_2 thin films have been published.[15-20] On the other hand, only a

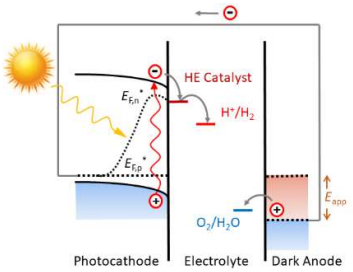

$$2H_2O \rightarrow 2H_2 + O_2 \qquad E^0 = -1.23\,V \text{ (eq. 1)}$$

$$2H^+ + 2e^- \rightarrow H_2 \qquad E^0 = 0\,V \text{ (eq. 2)}$$

$$2H_2O \rightarrow O_2 + 4H^+ + 4e^- \qquad E^0 = -1.23\,V \text{ (eq. 3)}$$

Figure 1. Top
this work bas
= fermi level
reaction (WS
evolution rea

tion used in
is (E_{app}). $E_{F,n}$* ter splitting and oxygen

[a] Institute of Chemical Research of Catalonia (ICIQ), The Barcelona Institute of Science and Technology, Avinguda Països Catalans 16, 43007 Tarragona, Spain. E-mail: cgimbert@iciq.cat; allobet@iciq.cat

[b] Catalonia Institute for Energy Research (IREC), Jardins de les Dones de Negre 1, 08930 Sant Adrià de Besòs, Spain.

[c] Departament de Química, Universitat Autònoma de Barcelona, 08193 Cerdanyola del Vallès, Barcelona, Spain.

Electronic Supplementary Information (ESI) available: optical characterization of the photoelectrodes, additional SEM images, electrochemical and photoelectrochemical experiments, J-V curve and EQE of equivalent PV device as well as additional details about experimental procedures. See DOI: 10.1039/x0xx00000x

few examples can be found in the literature where MoS_2 HER electrocatalyst is combined with semiconductors to build photocathodes.[21-24]

During the last decades, quaternary salts of the family of p-type kesterites with stoichiometry $Cu_2ZnSn(S/Se)_4$ have been widely used as photocathodes for the HER. They have been explored for their high performance as photoabsorbers in photovoltaic devices with efficiencies up to 12.7 % and V_{OC} up to 514 mV.[25] An additional attractive aspect of these materials is that they are made of non-critical raw materials and low-toxicity elements. The main family of kesterites that have been used in photoelectrochemistry for solar fuel production are those made of sulfur Cu_2ZnSnS_4, commonly abbreviated as CZTS. A pioneering work in this regard was published by Domen and coworkers in 2010. They used a CZTS photocathode with an additional n-type CdS layer to create a p-n junction, a TiO_2 top layer to protect the absorbers from the electrolyte and platinum nanoparticles on the surface to catalyse the HER.[26] In 2015, a modified electrode with an additional In_2S_3 inter-layer (Mo/CZTS/CdS/In_2S_3/Pt) and superior performance was reported by the same group.[27] Two years later, Luo, Zou and coworkers used a similar photocathode configuration improving the performance further with the addition of Ge.[28] More recently, selenium based thin-film kesterites have been tested as photocathodes containing a protecting top layer of TiO_2 and Pt catalyst on the surface.[29]

Despite all these promising advances, there is still a lack of an efficient and stable $Cu_2ZnSn(S/Se)_4$ photocathode that is made of inexpensive catalysts. In addition, the stability of the reported examples is most of the time an overlooked parameter that is critical for a possible market exploitation. In this work, CZTSe based p-type photoabsorbers are combined with MoS_2 electrocatalyst layers to build a powerful photocathode for the HER. The two key components have been selected for *i*) their high performance as light absorbers (CZTSe) and catalytic activity (MoS_2) and ii) for the optimum band alignment of the semiconductor[25,30,31] with the overpotential of the electrocatalyst,[12,14,18-20,22] that should favour charge separation and fast catalysis leading to high performance.

Experimental

Materials and methods

$(NH_4)_2[MoS_4]$ and Indium beads were supplied from Sigma-Aldrich. Mo/Cu/Sn/Cu/Zn stacks were sputtered using elemental targets of Mo (99.95%), Cu (99.99%), Zn (99.99%) and Sn (99.99%) supplied by PhotonExport. Ge nanolayers were thermally evaporated from Ge chips (99.999%) supplied by Sigma-Aldrich. The reactive annealings were performed using Se powder (99.999%, 200 mesh) and Sn powder (99.995%, 100 mesh) from Alfa Aesar. For the preparation of the CdS, $Cd(NO_3)_2$, $SC(NH_2)_2$, sodium citrate and ammonia from Alfa Aesar. The chemical etchings of the absorbers were performed using a $(NH_4)_2S$ (22% (w/w)) aqueous solution prepared from commercial $(NH_4)_2S$ (44% (w/w)) supplied by Alfa-Aesar. ZnO/ITO window layers were sputtered using ZnO (99.99%) and In_2O_3-SnO_2 (ITO) (99.99%) targets from PhotonExport.

UV-Vis measurements were carried out on a Lambda 1050 PerkinElmer spectrophotometer equipped with a PMT, InGaAs and PbS detectors system, double beam optics, double monochromator and D2 and W light sources. Diffuse reflectance measurements were carried out in the same equipment using 150mm Integrating Sphere with PbS and PMT detectors. Scanning electron microscopy (SEM) images were obtained with a ZEISS Series Auriga micro- scope using 5 kV accelerating voltage. External quantum efficiency (EQE) measurements were performed using a Bentham PVE300 system calibrated with Si and Ge photodiodes.

Commercially available glass coated ITO glasses (SPI supplies®) were cut in approximately 1,25 cm x 1,25 cm pieces and cleaned with 2% Hellmanex™ detergent, ethanol, acetone and dried under air flow. The electrical connection between copper wire and the electrode was made with solder (USS-9210 MBR electronics) using cerasolzer alloy (#CS186 MBR electronics). The electrical connection as well as the edges of the electrode were covered with non-transparent epoxy resin in order to isolate it from the solution. The electrode's area was calculated using J-Image (free software).

Linear sweep voltammetry (LSV) and Chronopotenciometry (CP) experiments were measured in a one compartment three electrode configuration cell with controlled illuminated area of 0.5 cm^2 using a CHI660D potentiostat. Platinum Disk/Mesh counter electrodes and reference electrodes (standard calomel electrode (SCE) or AgCl/Ag) were purchased from IJ-Cambria Ldt. Buffer solutions from pH 2 to pH 12 were prepared with H_3PO_4, NaH_2PO_4, Na_2HPO_4 and Na_2SO_4 from Sigma-Aldrich. Solutions at pH 13 were prepared with 0.1 M NaOH from Sigma-Aldrich. Photoelectrochemical experiments were ran under simulated 1 sun irradiation (100 mW/cm^2), using ABET 150LS Xenon lamps as a source of light provided with a AM1.5 filter. The irradiation intensity was calibrated with a Si photodiode.

A selective hydrogen Clark electrode (model H2-NP, Unisense) was used as a detector to quantify the amount of molecular hydrogen evolved from the (photo)electrodes during the photoelectrochemical experiment in a standard two-compartment cell separated with a frit.

Preparation of the multi-layered photoabsorber

The CZTSe films were prepared by a sequential process onto Mo-coated soda-lime glass substrates. For this purpose, Zn-rich and Cu-poor Cu/Sn/Cu/Zn stacks (Cu/(Zn+Sn) = 0.75 and Zn/Sn = 1.10 determined with calibrated X-ray fluorescence (Fischerscope XVD)) were deposited using DC magnetron sputtering (Alliance AC450). Additionally, very thin Ge layers were thermally evaporated prior to the stack deposition (10 nm Ge on the Mo) and on top of the metallic stack (5 nm Ge), as reported elsewhere.[32] Then, the whole precursor stack was subsequently annealed in a Se + Sn atmosphere (100 mg of Se and 5 mg of Sn), using graphite boxes (69 cm^3 in volume) in a conventional tubular furnace (Hobersal). The selenization was performed in a two-step process: the first one at 400 °C (heating

This journal is © The Royal Society of Chemistry 20xx

Please do not adjust margins

rate of 20 °C/min) for 30 minutes and 1.5 mbar of argon pressure, followed by a second step at 550 °C (heating rate of 20 °C/min) for 15 minutes and 1 bar of Ar pressure, with a natural cooling down to room temperature. To complete the devices, a CdS buffer layer (50 nm) was grown by chemical bath deposition, preceded by a chemical etching in $(NH_4)_2S$ solution in order to remove possible secondary phases and to passivate the absorbers surface. Just after CdS growth, the multilayered photoabsorber were completed by DC-pulsed sputtering deposition of ZnO (50 nm) and In_2O_3-SnO_2 (ITO, 200 nm) as transparent conductive window layer (Alliance CT100).

(Photo)electrodeposition of the MoS_2 electrocatalyst

An electrochemical bath containing 30mM of $(NH_4)_2[MoS_4]$ and 0.1M Na_2SO_4 as supporting electrolyte in MilliQ water was used for both electrodeposition on commercially available ITO glasses and photoelectrodeposition on the CZTSe absorbers. The solution was kept under argon bubbling during the whole experiment to prevent the formation of molybdenum oxides and used as prepared. In a standard experiment, the potentiostat was set to galvanostatic mode at $j = -7.5 \cdot 10^{-5}$ A/cm^2 to cathodically electroplate the amorphous MoS_2. The thickness of the catalyst layer is controlled by the time and charge passed through the system during the electrodeposition. In a typical experiment, a loading corresponding to a charge of 0.05 C/cm^2 was performed, which corresponds to a 200 nm of thickness approximately (confirmed by SEM). After the electrodeposition, the electrodes were cleaned with MilliQ water and dried under air flow.

An analogous methodology was used for the CZTSe electrodes functionalization. Before making the electrical contact with indium as soldering material, the four edges of the photoelectrode were scratched, removing the material to expose the molybdenum back contact (approximately 0.5-1 mm of wideness). The photoelectrochemical deposition was done under irradiation with a light intensity calibrated to 2 suns due to the high concentration of the dark red coloured $(NH_4)_2[MoS_4]$ solution.

Photo-electrochemical experiments

In a custom-made one-compartment, three-electrode configuration cell made of Teflon with a 0.5 cm^2 window, the working CZTSe electrode, platinum counter electrode and reference electrode were placed close together inside the buffered solution. Prior to the electrochemical experiment, the solution is degassed by bubbling argon for 20 min. LSV, CP and/or bulk electrolysis experiments were performed under continuous light irradiation calibrated to 1 sun (100 mW/cm^2).

For detection of hydrogen gas, a two-compartment cell made of glass and separated by a frit was used. The working CZTSe electrode was placed together with the AgCl/Ag reference electrode in one compartment, while the platinum mesh was placed in the second compartment facing as close to the frit as possible. After degassing the solution with argon flow, the CP experiment is started and the evolved hydrogen gas monitored with a Clark sensor in the headspace of the cathodic compartment.

Results en discussion

Preparation of CZTSe absorber layer

The photoabsorber consists of a carefully designed multilayered configuration that can be formulated as Mo/$MoSe_2$/$Cu_2ZnSnSe_4$/CdS/ZnO/ITO (where ITO is indium tin oxide). The n-type CdS interlayer has been proved to be crucial for device performance by creating a very efficient p-n junction with the p-type CZTS(Se) type of absorbers.[26](REF) On the other hand, ZnO fills the defects of the CdS layer that is prepared by chemical bath deposition as described below. It also gives a uniform support for the deposition of the ITO protecting layer. Detailed description of the preparation of the samples is given in the supporting information.[32,33,34] Briefly, it consists of selenization of Cu/Zn/Sn stacks, that have been previously deposited by sputtering on molybdenum-coated soda-lime glass (also prepared by sputtering). The resulting Mo/$MoSe_2$/$Cu_2ZnSnSe_4$ samples are dipped in a chemical bath for n-type CdS deposition, followed by the sputtering deposition of ZnO and ITO in order to complete the electrode configuration. Finally, the device is subjected to a soft post-deposition annealing at 250 °C for 15 minutes on a hotplate in air atmosphere to improve cathode performance. The full photoabsorber Mo/$MoSe_2$/$Cu_2ZnSnSe_4$/CdS/ZnO/ITO will be regarded as CZTSe hereafter. Powder x-ray diffraction, resonance Raman spectroscopy and transmission electron microscopy analysis of the prepared samples confirmed the crystallinity and purity of the $Cu_2ZnSnSe_4$ photoabsorber layer with no secondary phases (Figures SX and SY in the supporting information). Composition, morphology and grain size were also as previously reported.[29,33] Optical band gap of the four absorbing layers CZTSe/CdS/ZnO/ITO were measured using UV-VIS diffuse reflectance spectroscopy (DRS) and external quantum efficiency (EQE) experiments obtaining the expected values according to the literature (Figure S1 and Table S1 in the SI).[35,36] In Figure S1, a representative Tauc plot obtained from DRS spectrum shows seven transitions corresponding to CZTSe (pure, E_g =0.94 eV), CZTSSe (E_g =1.35 eV), two for CdS (E_g =2.1-2.0 eV), two for ZnO/ZnS (E_g =3.0-3.4 eV)[37] and one for ITO (E_g = 2.9 eV). Due to the post deposition annealing, some S^{2-} migrate from CdS to ZnO and CZTSe layers, doping the absorber, as well as Cu^+ ions doping CdS layer, phenomena that have proven to be beneficial for the device efficiency.[38] Thus, CdS and ZnO feature double peaks (green dashed lines in Figure S1), very likely due the shallow doping during the post deposition annealing, thus corresponding one to the pure material and the other to the doped material

Optimization of the MoS_2 electrocatalyst layer

Molybdenum sulfide MoS_x (x = 2 or 3) can be prepared by electrodeposition from the precursor $(NH_4)_2[MoS_4]$ into conductive substrates in three different ways: i) cathodic deposition, ii) anodic deposition and iii) cyclic deposition.[15-17] The last two approaches were ruled out due to the required

Please do not adjust margins

Please do not adjust margins

xidation potential, which could lead to the chemical decomposition of the CZTSe absorber during the photoelectrochemical deposition. Thus, in this work, we focused on the cathodic deposition approach, which we performed from the precursor $(NH_4)_2[MoS_4]$ (30 mM) on ITO in galvanostatic mode (j = -7.5·10^{-5} A/cm^2). The process was done under weak argon bubbling to avoid the formation of molybdenum oxides. The loading of the molybdenum sulfide deposited on the surface of ITO was controlled by the total amount of charge passed through the electrochemical system. The performance of the resulting MoS_2-coated ITO electrodes (ITO-MoS_2 hereafter) towards HER in pH 2 phosphate buffer solution with different loadings of the electrocatalyst is summarized in Table 1 (see also Figure S2-S3 in the SI). The overpotential required to reach -1 mA/cm^2 decreases with increasing amount of MoS_2 while the current density at E = -0.3V *vs* RHE increases with higher amount of catalyst. The MoS_2 films are not transparent and therefore are expected to influence the light absorbing process once deposited on the CZTSe photoabsorber (Figure S4). Thus, although the best performing electrode is that with a charge loading of 0.1 C/cm^2, it is also the electrode with a lower degree of transmittance (10-55 % in the range of 350-800nm). Therefore, the ITO-MoS_2 electrode with Q = 0.05 C/cm^2 with E = -0.175 V at j =-1 mA/cm^2 and j = -9.46 mA/cm^2 at E = -0.3 V was selected as a good compromise between high activity and high transparency (Figure 2).

The ITO-MoS_2 electrodes show a reduction process at potentials between -0.025 and -0.150 V *vs* RHE, before the hydrogen evolution reaction, attributed to the reduction of the MoS_3 to MoS_2 during the first Linear Sweep Voltammetry (LSV) scan.[15,17] This reduction wave was not observed again in subsequent scans of the LSV experiments on the same sample (Figure 2, compare red and blue traces). The activity of the ITO-MoS_2 electrodes is highly dependent on the pH of the electrolyte solution, showing drastic decrease of the cathodic current associated to the HER in pH values higher than 2 (Figure S5). ITO-MoS_2 electrodes tested in pH higher than 10 were unstable and the catalyst peeled off very quickly from the electrode surface. This result is in sharp contrast to other reported amorphous MoS_2 based electrodes for HER in the literature which are very active in extreme pH values (0 and 14).[39] We attribute these results to the lower adhesion of our MoS_2 to the ITO substrate.

Table 1. Overpotential (at j = -1 mA/cm^2) and current density (at η = 300 mV) values of the ITO-MoS_2 samples with different loadings of HER catalyst.

Charge (C/cm^2)	E for j = -1 mA/cm^2	j at $E_{vs\ RHE}$ = -0.3 V
0.01	-0.205 V	-7.37 mA/cm^2
0.02	-0.195 V	-8.45 mA/cm^2
0.05	-0.175 V	-9.46 mA/cm^2
0.1	-0.165 V	-9.96 mA/cm^2

LSV experiments in Figure 2 show that ITO-MoS_2 electrodes with a 0.05 C/cm^2 loading feature an overpotential of -175 mV and -330 mV *vs* RHE to reach -1 mA/cm^2 and -10 mA/cm^2 respectively at pH 2. A chronopotentiometry (CP) experiment at -10 mA/cm^2

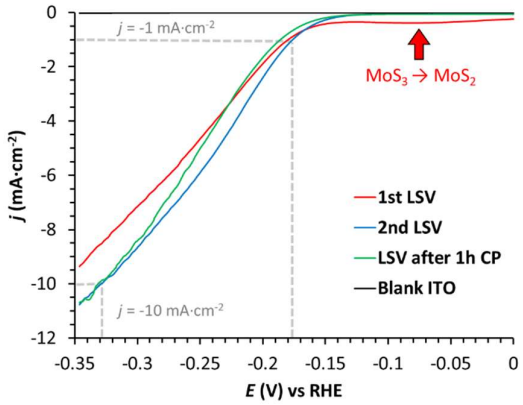

Figure 2. LSV of ITO-MoS_2 with a Q = 0.05 C/cm^2 loading at pH 2. Counter electrode: Pt mesh. Reference electrode: AgCl/Ag. Scan rate: 5 mV/s. Experiments recorded under stirring conditions. *i*R drop corrected at 85%.

was ran for 1 hour, showing no significant loss of activity (Figure 3). The averaged overpotential required to sustain -10 mA/cm^2 for the whole experiment was -328 mV *vs* RHE, in good agreement with the LSV results in Figure 2 and indicating that the scan rate used to run the LSV was close to stationary conditions. In order to check the Faradaic efficiency (FE), the experiment was repeated in a two-compartment electrochemical cell, monitoring the amount of hydrogen evolved from the cathode by using a Clark electrode sensor, obtaining 100% efficiency (Figure 3, inset). The activity of the electrode after this test was also checked by LSV without remarkable losses of current densities (Figure 2, compare blue and green traces). Long-term CP tests up to 10h were ran to assess the stability of the ITO-MoS_2 electrodes. The catalytic activity started to decrease linearly after 1 hour of electrolysis until the 5th hour. At this time the required potential to run j = -10 mA/cm^2 is E = -0.6 V as opposed to the E = -0.33 V required during the first hour (Figure S6). After 5h, the HER activity of the

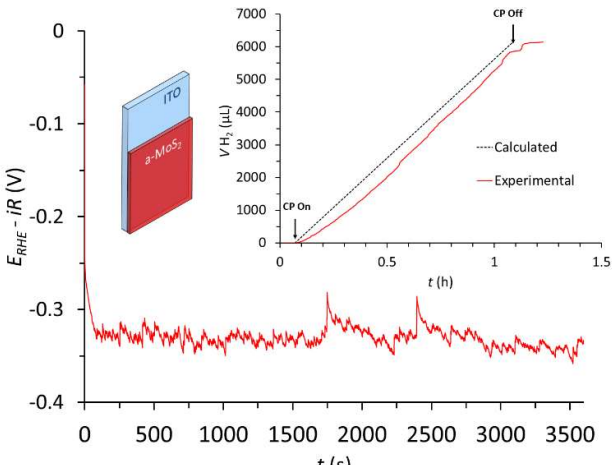

Figure 3. CP of ITO-MoS_2 with a Q = 0.05 C/cm^2 loading in pH 2 at -10mA/cm^2 in a two-compartment electrochemical cell. Counter electrode: Pt mesh. Reference electrode: AgCl/Ag. *i*R drop corrected at 85%. *Inset:* Amount of molecular hydrogen evolved during CP experiments (red line) and the calculated from the charged passed (black dotted line).

This journal is © The Royal Society of Chemistry 20xx

Please do not adjust margins

electrode decreases drastically requiring even lower potentials to sustain the selected current density.

In order to get insights into the deactivation processes during electrolysis, the morphology of the electrodes before and after catalysis were analyzed by Scanning Electronic Microscopy (SEM). Top view SEM images confirm homogeneous and continuous MoS_2 films covering completely the ITO surface after deposition of the electrocatalyst (Figure 4A and Figure S7). Only small cracks in the amorphous MoS_2 layer can be observed, that are likely produced by the mechanical stress due to the expansion of hydrogen bubbles formed during the electrodeposition process. After 1h of electrolysis, the SEM images show small regions where the initial cracks start to get wider, starting to expose the ITO underlayer to the electrolyte (Figure 4B). The cracks become even larger after 10h of experiment when the ITO is mostly exposed and only little amount of the MoS_2 layer is left accounting for the loss in activity at long electrolysis time (Figure 4C). Interestingly, the shape of some of the cracks suggest a peeling due to mechanical stress from a gas bubble rather than a chemical process (Figure S8). It is important to notice that the images of the damaged regions shown in Figure 4B and 4C were chosen from the most affected zones and they are not representative of the whole surface, where the ITO-MoS_2 mainly looks intact (Figure S9).

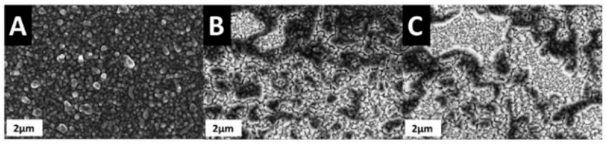

Figure 4. Top view SEM images of ITO-MoS_2 electrodes as prepared (A), after 1h of CP (B) and after 10h of CP (C).

MoS_2 modified CZTSe and HER photoelectrochemical performance

The CZTSe absorbers were functionalized with MoS_2 by cathodic photoelectrodeposition onto the ITO top layer in galvanostatic mode (j = -7.5·10^{-5} A/cm^2) under 2 sun illumination due to the strong absorption of light by the electrochemical bath containing 30 mM of the red precursor $(NH_4)_2[MoS_4]$. This methodology resulted to be a very useful way to get consistent rate of growth of the catalyst film despite the fact that the actual applied potential to make the HER catalyst layer growth is different due to the slightly distinct photovoltage generated by different samples of CZTSe. This is exemplified in Figure S10, which shows the *E-t* curves of MoS_2 deposition from representative ITO and CZTSe (photo)electrodes. The catalyst deposition using this method is very reproducible, giving identical *E-t* curves for ITO samples and only slight differences in *E-t* curves for the CZTSe samples.

The photoelectrochemical activity towards HER of the CZTSe-MoS_2 electrodes was tested in pH 2 phosphate buffer solution under 1 sun illumination. Analogous to the ITO-MoS_2 electrodes, the CZTSe-MoS_2 photocathodes also showed a reduction process before the HER catalysis assigned to the MoS_3 to MoS_2 transformation at potentials from 0.4 to 0.25 V *vs* RHE during the first LSV scan (Figure S11). As depicted in the red line of Figure 5, CZTSe covered with MoS_2 features an onset potential and overpotential of +254 mV and +100 mV to achieve -1 mA/cm^2 and -10 mA/cm^2 respectively (see also Figure S12). No dark-current was observed in the range of potentials used as indicated with the red dashed line in Figure 5. Due to the high overpotential required to produce molecular hydrogen for raw CZTSe photocathode no photocurrent was detected below 0 V *vs* RHE without the MoS_2.

By comparing the LSV of the ITO-MoS_2 and the CZTSe-MoS_2 electrodes we can observe the onset potential for HER is anodically shifted by approximately +430 mV (Figure 5). This value is close to the Open Circuit Potential (V_{oc} = 464 mV) obtained from the *J-V* curve of an equivalent photovoltaic device, indicating minimum losses in photovoltage (V_{ph}) by the presence of the MoS_2 layer, and suggesting we are at the limit of the capabilities of the photoabsober (Figure S13). In addition, the similarity of the catalytic slopes of the two electrodes indicates that the same species (MoS_2) is responsible for the chemical reaction (compare blue and red lines in Figure 5). Remarkably, the high current densities obtained for our CZTSe-MoS_2 electrode are amongst the best performing photocathodes for the hydrogen evolution reaction described in the literature (Table S2). While the sulfur containing kesterite based photoelectrodes (CZTS) give higher photovoltages due to their larger band gap, their current densities are significantly lower than those of the CZTSe described in this work (below -10 mA/cm^2 for the former as opposed to the -18 mA/cm^2 for the latter at E = 0 V vs RHE.[26-28,40,41] Another important advantage of our photoelectrodes is the use of a more readily available MoS_2 catalyst as opposed to the Pt based CZTS(Se) examples reported to date.[29] In this regard, previous works using similar electrocatalytic MoS_2 layers but different semiconductor materials such as Cu_2O show lower performance in terms of current densities and stability.[39] Only those photocathodes that use p-Si modified with MoS_2 give comparable results.[21-24]

CP experiments at -10 mA/cm^2 were ran in a two-compartment cell under 1 sun illumination, obtaining an averaged potential of +86 mV *vs* RHE for one hour with FE of 100% and no significant loss in activity (Figure 6 and S14). A LSV experiment of the

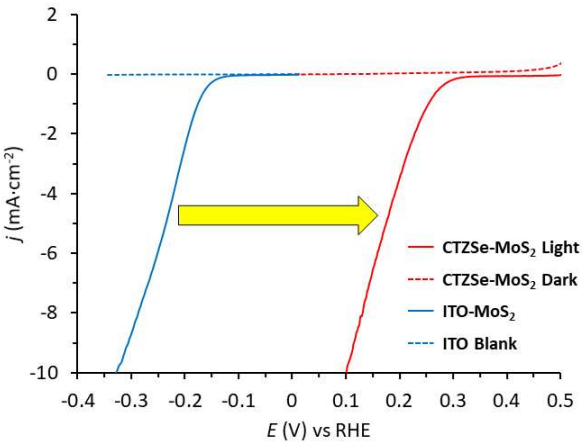

Figure 5. LSV of ITO-MoS_2 and CZTSe-MoS_2 with the same loading of catalyst. Scan rate: 5 mV/s. LSV recorded under stirring conditions. *i*R drop corrected at 85%.

photocathode after CP shows a slight decrease in activity requiring an overpotential of +233 mV and +66 mV to get -1 mA/cm^2 and -10 mA/cm^2 respectively (Figure S12, compare red and blue lines). Longer CP experiments show that our photocathode is able to produce molecular hydrogen at -10 mA/cm^2 for 2h without any significant loss in activity (*i.e.* 1.2 µL(H_2)/cm^2·s) and able to perform HER below the thermodynamic potential for 3.5 hours (Figure S16). After the first two hours, the potential required to sustain -10 mA/cm^2 increases linearly, increasing the potential by *ca.* 44 mV/h, a similar trend that was observed for the ITO-MoS_2 electrodes. Interestingly, the MoS_2 layer seems to last longer when it is on the surface of the photoelectrode (2h) than when it is on the ITO electrode (1h). This result might be attributed to the distinct nature of the ITO surface when it is deposited on top of the CZTSe/CdS/ZnO photoabsorber compared to when it is deposited directly onto the glass, resulting in better adhesion to the surface in the former case.

Due to the low stability of the ITO layer directly immersed in pH 2,[42-44] it was not possible to measure more than two scans with raw CZTSe because of the fast degradation of the photoabsorber. Thus, the amorphous MoS_2 layer not only reduces the overpotential for HER, but also protects the ITO and the absorber layers from the electrolyte, preventing its corrosion and dissolution. This is also supported by aging experiments consisting of immersing the CZTSe-MoS_2 photoelectrodes in pH 2 for 5 hours, showing no change in activity (Figure S17). Therefore, the loss of activity is attributed to the depletion of electroactive material during catalysis most likely due to mechanical stress from the evolution of H_2 bubbles, as suggested also for the parent ITO-MoS_2 electrodes.

SEM images of the CZTSe-MoS_2 electrodes show the homogeneity and compactness of the top layer before and after catalytic tests, despite the small cracks already mentioned for the analogous ITO-MoS_2 (Figure 7, A and D). While the top-view SEM images did not show any change in the morphology, cross-sections of the photocathodes as prepared and after 1 hour of CP revealed that the MoS_2 layer became thinner (Figure 7, D and E) from 150-250 nm to 80-130 nm. The electrocatalyst layer became even thinner with the extended CP, reaching 60-90nm

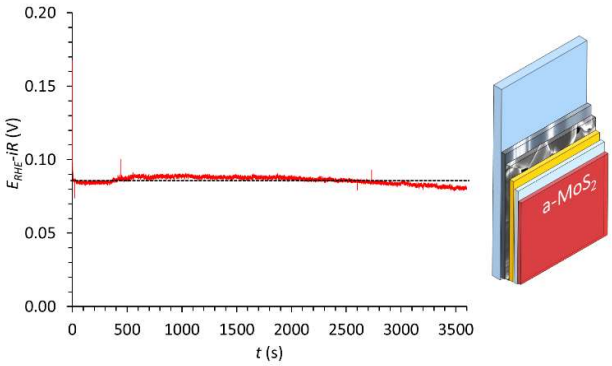

Figure 6. **Left)** CP of CZTSe-MoS_2 in pH 2 at -10 mA/cm2 in a two-compartment photoelectrochemical cell. Dashed black line indicates the averaged potential during the CP experiment (E = +86 mV). **Right)** Schematic drawing of the CZTSe photoelectrode where a-MoS_2 is amorphous molybdenum disulfide.

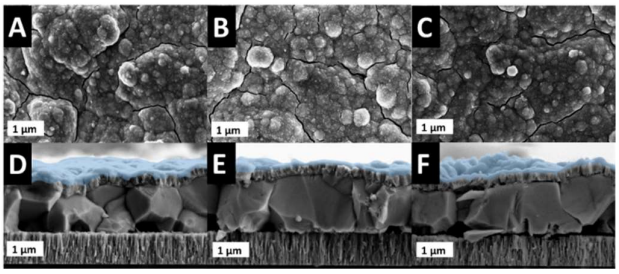

Figure 7. Top view and cross section of SEM images of CZTSe-MoS_2 as prepared (A and D), after 1h of CP (B and E) and after 5h (C and F). In cross-section images, MoS_2 layer was coloured with blue.

of thickness after 5 hours. No peeled regions were found during the surface analysis as opposed to what was observed for the ITO-MoS_2 electrodes suggesting that the mechanical stability in this case is better. On the other hand, the other layers (Mo/$MoSe_2$/CZTSe/ZnO/ITO) look intact, highlighting once more the stabilizing role of the MoS_2 electrocatalytic layer.

Conclusions

A simple and easily scalable method based on galvanostatic (photo)deposition of MoS_2 from $(NH_4)_2[MoS_4]$ has been developed giving excellent and reproducible results on the surface of conductive supports (ITO) or on the surface of a multilayered absorber based on p-type kesterite CZTSe (Mo/$MoSe_2$/$Cu_2ZnSnSe_4$/CdS/ZnO/ITO).

The resulting CZTSe-MoS_2 photoelectrodes show impressive HER catalytic performance at pH 2 with current densities up to -18 mA/cm^2 at E = 0 V vs RHE and sustained catalysis at +86 mV *vs* RHE at j = 10 mA·cm^{-2}. A comparison with its analogous dark electrode ITO-MoS_2 allows us to calculate a photovoltage of 430 mV. This value is in good agreement with the V_{OC} = 464 mV of a photovoltaic device made of the same absorber, indicating that our system takes advantage of the full photoabsorption capabilities of the CZTSe material. In addition, the stability of the CZTSe-MoS_2 photocathodes has been studied in detail, finding that it is able to perform HER for two hours without any significant loss of activity. Moreover, it is able to keep the hydrogen production for more than 3.5 hours below the thermodynamic potential (E = 0 V *vs* RHE). Longer reaction times induce loss of the electroactive layer caused by the expansion of microbubbles on the surface of the photocathode as demonstrated by SEM images. A similar phenomenon has been observed for the analogous dark ITO-MoS_2 electrodes. In sharp contrast, the photoactive CZTSe layer remains intact, highlighting the key role of the MoS_2 film in isolating it from the electrolyte. All these results allow us to conclude that, amorphous MoS_2 obtained by (photo)electrodeposition is a very good catalyst for HER, inexpensive and easy to prepare that not only reduces the overpotential for HER but also protects the sensitive photoactive underlayers of the photocathode from the corrosive catalytic media. According to these findings, future endeavors should be focused on improving the adhesion between the electrocatalyst MoS_2 layer and the photoabsorber.

This journal is © The Royal Society of Chemistry 20xx

Please do not adjust margins

Conflicts of interest

"There are no conflicts to declare".

Acknowledgements

Support from MINECO, FEDER, AGAUR and H2020 Programme are gratefully acknowledged through grants CTQ2016-80058-R, CTQ2015-73028-EXP, SEV 2013-0319, ENE2016-82025-REDT, CTQ2016-81923-REDC, 2017-SGR-1631, 2017-SGR-862, ENE2016-80788-C5-1-R, ENE2017-87671-C3-1-R, BES-2014-068533, and H2020-NMBP-03-2016-720907.

Notes and references

1 BP Statistical Review of World Energy. Statistical Review of World Energy June 2018; BP p.l.c., 1 St James's Square, London, SW1Y 4PD, UK, 2018.
2 IEA. Global Energy & CO_2 Statuts Report; 2018.
3 J. Barber, *Chem. Soc. Rev.* 2009, **38**, 185.
4 N. S. Lewis, *Science* 2016, **351**, aad1920.
5 M. G. Walter, E. L. Warren, J. R. Mckone, S. W. Boettcher, Q. Mi, E. A. Santori, N. S. Lewis, *Chem. Rev.* 2010, **110**, 6446.
6 M. S. Prévot, K. Sivula, *J. Phys. Chem. C* 2013, **117**, 17879.
7 S. D. Tilley, *Adv. Energy Mater.* 2019, **9**, 1802877.
8 K. Sivula, R. van de Krol, *Nature Rev. Mater.* 2016, **1**, 15010.
9 M. Saurat, S. Bringezu, *J. Ind. Ecol.* 2008, **12**, 754A.
10 E. Alonso, E.; F. R. Field, R. E. Kirchain, *Environ. Sci. Technol.* 2012, **46**, 12986.
11 I. Chorkendorff, I. K. P. JørgensenJ. H. Nielsen, B. Hinnemann, B. P. G. Moses, J. K. Nørskov, S. Horch, J. Bonde, *J. Am. Chem. Soc.* 2005, **127**, 5308.
12 G. Li, D. Zhang, Q. Qiao, Y. Yu, D. Peterson, A. Zafar, R. Kumar, S. Curtarolo, F. Hunte, S. Shannon, Y. Zhu, W. Yang, L. Cao, *J. Am. Chem. Soc.* 2016, **138**, 16632.
13 Z. He, W. Que, *Appl. Mater. Today* 2016, **3**, 23.
14 I. Chorkendorff, J. Bonde, K. P. Jorgensen, S. Horch, T. F. Jaramillo, J. H. Nielsen, Science 2007, **317**, 100.
15 H. Vrubel, X. Hu, *ACS Catal.* 2013, **3**, 2002.
16 D. Merki, S. Fierro, H. Vrubel, X. Hu, *Chem. Sci.* 2011, **2**, 1262.
17 C. G. Morales-Guio, X. Hu, *Acc. Chem. Res.* 2014, **47**, 2671.
18 A. Albu-Yaron, C. Lévy-Clément, A. Katty, S. Bastide, R. Tenne, *Thin Solid Films* 2000, **361**, 223.
19 E. A. Ponomarev, G. Hodes, *Thin Solid Films* 1996, **280**, 186.
20 Y. Huang, R. J. Nielsen, W. A. Goddard, M. P. Soriaga, *J. Am. Chem. Soc.* 2015, **137**, 6692.
21 L. A. King, T. R. Hellstern, J. Park, R. Sinclair, T. F. Jaramillo, *ACS Appl. Mater. Interfaces* 2017, **9**, 36792.
22 M. J. Shearer, S. Jin, Q. Ding, D. Liang, M. Cabán-Acevedo, A. S. Daniel, C. R. English, F. Meng, R. J. Hamers, *J. Am. Chem. Soc.* 2014, **136**, 8504.
23 C. G. Morales-Guio, K. Thorwarth, B. Niesen, L. Liardet, J. Patscheider, C. Ballif, X. Hu, *J. Am. Chem. Soc.* 2015, **137**, 7035.
24 K. C. Kwon, S. Choi, K. Hong, C. W. Moon, Y.-S. Shim, D. H. Kim, T. K. W. Sohn, J.-M. Jeon, C.-H. Lee, K. T. Nam, S. Han, S. Y. Kim, H. W. Jang, Energy Environ. Sci. 2016, **9**, 2240.
25 Dhawale, D. S.; Ali, A.; Lokhande, A. *Sustain. Energy Fuels* 2019, **3**, 1365.
26 D. Yokoyama, T. Minegishi, K. Jimbo, T. Hisatomi, G. Ma, M. Katayama, J. Kubota, H. Katagiri, K. Domen, *Appl. Phys. Express* 2010, **3**, 2.
27 F. Jiang, Gunawan, T. Harada, Y. Kuang, T. Minegishi, K. Domen, S. Ikeda, *J. Am. Chem. Soc.* 2015, **137**, 13691.
28 X. Wen, W. Luo, Z. Guan, W. Huang, Z. Zou, *Nano Energy* 2017, **41**, 18.
29 C. Ros, T. Andreu, S. Giraldo, V. Izquierdo-Roca, E. Saucedo, J. R. Morante, *ACS Appl. Mater.* Interfaces 2018, **10**, 13425.
30 S. Chen, L. W. Wang, *Chem. Mater.* 2012, **24**, 3659.
31 R. Haight, A. Barkhouse, O. Gunawan, B. Shin, M. Copel, M. Hopstaken, D. B. Mitzi, *Appl. Phys. Lett.* 2011, **98** (25), 253502.
32 S. Giraldo, E. Saucedo, M. Neuschitzer, F. Oliva, M. Placidi, X. Alcobé, V. Izquierdo-Roca, S. Kim, H. Tampo, H. Shibata, A. Pérez-Rodríguez, P. Pistor, *Energy Environ. Sci.* 2018, **11**, 582.
33 M. Neuschitzer, E.-R. Moises, M. Guc, J. Prieto, S. Giraldo, I. Forbes, P.-R. Alejandro, E. Saucedo, *J. Mater. Chem.* 2018, **6**, 11759.
34 S. Giraldo, M. Neuschitzer, T. Thersleff, S. López-Marino, Y. Sánchez, H. Xie, M. Colina, M. Placidi, P. Pistor, V. Izquierdo-Roca, V.; K. Leifer, A. Pérez-Rodríguez, E. Saucedo, *Adv. Energy Mater.* 2015, **5**, 1501070.
35 K. Kaur, N. Kumar, M. Kumar, *J. Mater. Chem. A* 2017, **5**, 3069.
36 S. Li, S.; C. Ghinea, T. J. M. Bayer, M. Motzko, R. Schafranek, A. Klein, *J. Phys. Condens. Matter* 2011**, 23**, 33.
37 A. Torabi, V. N. Staroverov, *J. Phys. Chem. Lett.* 2015, **6**, 2075.
38 M. Neuschitzer, Y. Sanchez, T. Olar, T. Thersleff, S. López-Marino, F. Oliva, M. Espindola-Rodríguez, H.; Xie, M. Placidi, V. Izquierdo-Roca, I. Lauermann, K. Leifer, A. Pérez-Rodríguez, E. Saucedo, *Chem. Mater.* 2015, **27**, 5279.
39 C. G. Morales-Guio, L. Liardet, M. T. Mayer, S. D. Tilley, M. Grätzel, X. Hu, *Angew. Chem. Int. Ed.* 2015, **54**, 664.
40 K. Wang, D. Huang, L. Yu, H. Gu, S. Ikeda, F. Jiang, *J. Colloid Interface Sci.* 2019, **536**, 9.
41 L. Rovelli, S. D. Tilley, K. Sivula, *ACS App. Mater. Interfaces* 2013, **5**, 8018.
42 M. Senthilkumar, J. Mathiyarasu, J. Joseph, K. L. N. Phani, V. Yegnaraman, *Mater. Chem. Phys.* 2008, **108**, 403.
43 J. D. Benck, B. A. Pinaud, Y. Gorlin, T. F. Jaramillo, *PLoS One* 2014, **9,** 10.
44 S. Geiger, O. Kasian, A. M. Mingers, K. J. J. Mayrhofer, S. Cherevko, *Sci. Rep.* 2017, **7**, 1.

Please do not adjust margins

"This document is the Accepted Manuscript version of a Published Work that appeared in final form in Journal of Materials Chemistry A, copyright © The Royal Society of Chemistry 2019 after peer review and technical editing by the publisher. To access the final edited and published work see:

https://pubs.rsc.org/en/content/articlelanding/2019/ta/c9ta08818k#!divAbstract

Table of Contents

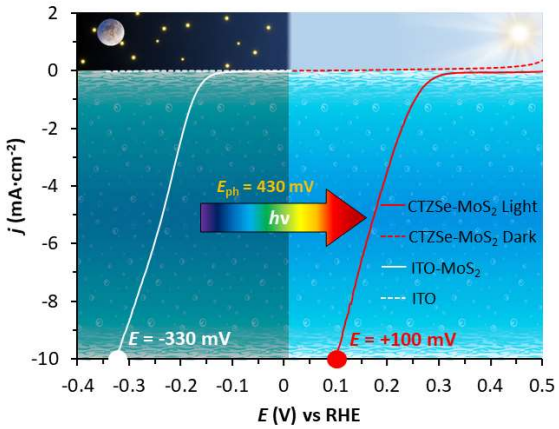

Key words
Hydrogen evolution, photocathode, kesterite, molybdenum disulphide, photoelectrochemical cell